

## Perforation optimization of hydraulic fracturing of oil and gas well

Hai Yan Zhu<sup>1,2a</sup>, Jin Gen Deng<sup>\*1</sup>, Zi Jian Chen<sup>1</sup>, Feng Chen An<sup>2</sup>,  
Shu Jie Liu<sup>3</sup>, Cheng yong Peng<sup>3</sup>, Min Wen<sup>3</sup> and Guang Dong<sup>4</sup>

<sup>1</sup> State Key Laboratory of Petroleum Resource and Prospecting  
(China University of Petroleum), Beijing 102249, China

<sup>2</sup> School of petroleum engineering, Southwest Petroleum University, Chengdu, Sichuan 610500, China

<sup>3</sup> School of Engineering and Electronics, Edinburgh University, Edinburgh EH9 3JN, UK

<sup>4</sup> CNOOC Research Institute, Beijing 100027, China

<sup>5</sup> Research Institute of Engineering and Technique, Huabei Sub-Company,  
SINOPEC, Zhengzhou, Henan 450006, China

(Received December 19, 2012, Revised April 14, 2013, Accepted May 23, 2013)

**Abstract.** Considering the influences of fluid penetration, casing, excavation processes of wellbore and perforation tunnels, the seepage-deformation finite element model of oil and gas well coupled with perforating technique is established using the tensile strength failure criterion, in which the user-defined subroutine is developed to investigate the dynamic evolvement of the reservoir porosity and permeability. The results show that the increases of perforation angle and decreases of perforation density lead to a higher fracture initiation pressure, while the changes of the perforation diameter and length have no evident influences on the fracture initiation pressure. As for initiation location for the fracture in wellbore, it is on the wellbore face while considering the presence of the casing. By contrast, the fractures firstly initiate on the root of the tunnels without considering casing. Besides, the initial fracture position is also related with the perforation angle. The fracture initiation position is located in the point far away from the wellbore face, when the perforation angle is around 30°; however, when the perforation angle is increased to 45°, a plane fracture is initiated from the wellbore face in the maximum horizontal stress direction; no fractures was found around perforation tunnels, when the angle is close to 90°. The results have been successfully applied in an oilfield, with the error of only 1.1% comparing the fracture initiation pressure simulated with the one from on-site experiment.

**Keywords:** perforation parameters; finite elements; initiation pressure; hydraulic fracturing

### 1. Introduction

Hydraulic fracturing is a newly developed technique to stimulate oil production from the wells in declining oil reservoirs, which is done after a well is drilled by injecting large volumes of water, sand (other propping agent) and specialized chemicals under enough pressure to fracture the formations holding the oil. The sand or other proppants are left in the fracture after its formation,

---

\*Corresponding author, Professor, E-mail: dengjingen@126.com

<sup>a</sup> Ph.D., E-mail: zhuhaiyan040129@163.com

holding the fractures open to allow the oil to flow freely out of the formation and into a production well. With technological advances, hydraulic fracturing is now widely used to initiate and stimulate oil production in the unconventional oil and gas formations with low permeability that was inaccessible before. Its application, along with horizontal drilling, for production of natural gas (methane) and oil from tight sands, unconventional shale formations and other unconventional reserves, has been enabling the expansion of gas reserves and the development of tight oil resources, such as Bakken and Eagle Ford Formation. In the meantime, this technique could help decrease the surface density of wells in an area with low permeability, since that more wells need to be drilled into reservoir than into more permeable, conventional reservoir to retrieve the same amount of oil.

However, it is very difficult for professionals to find a suitable instrument to gauge the fracture initiation pressure for the well, to control the injection fluid pressure. In view of that, researchers in the field turned to various simulations to predict its fracture initiation, through the criterion that the tensile stress exceeds the tensile strength of rock. During the process of hydraulic fracturing, it is the injection fluid that has directly caused the tunnel wall to fracture, so the seepage-deformation coupling mechanics needs to be adopted to do the analysis of the rock stress around the tunnel wall. The predicted model of the fracture initiation pressure based on a single perforation tunnel is proposed and verified by Daneshy (1973), Pearson *et al.* (1992), Abass *et al.* (1994), Hossain *et al.* (2002), Crosby *et al.* (2002), Soliman and Boonen (2002), Osorio and Lopez (2009), Fallahzadeh *et al.* (2010). However, it failed to give the optimum parameters of the perforation tunnels, since that there is no consideration of the interplaying effects of the adjacent perforation tunnels.

Of course, there are many researchers who have considered interplaying effects with multiple holes under internal and external pressures while doing the investigation of stress concentration problem, but it is solved as plane problem (Wang and Lin 1998) and impossible to be used in the seepage-deformation coupling situation, let it alone that investigating the stress under 3D conditional state. Similarly, Zhang *et al.* (2003) had done the simulation of the vertical perforation using ANSYS, through doing the parameters analysis, including the perforation angle (the angle between the perforation direction and the maximum horizontal stress), the perforation diameter, the perforation density and length, etc. Biao *et al.* (2011) studied the influences of the different perforation densities and styles on the rock initiation during the spiral perforating of the vertical well. In sum, the main purpose of the studies mentioned above is to observe the influences of the perforation parameters on the hydraulic fracturing of the vertical well with the consideration of the casing or the fluid penetration.

In our study, the influences of different perforation parameters on the hydraulic fracturing of oil and gas well by finite element method (FEM) were selected to do the analysis in FEM modelling, by considering the influences of the fluid penetration, the casing, the excavation processes of the wellbore and the perforation tunnels. The main purpose of the study is to find a way to more accurate prediction in FEM modeling, and provide a more reliable, practical and economical guidance to the design of the hydraulic fracturing of oil and gas well in the near future.

## **2. Hydraulic fracturing model of oil and gas well**

### *2.1 Hydraulic fracturing initiation pressure of a single perforation tunnel*

The rock in this study is a homogeneous and linear elastic porous material, the stress

distribution around the wellbore is considered as a plain strain problem. The coordinate system 1/2/3 is accordant with the direction of the  $\sigma_v$ ,  $\sigma_H$  and  $\sigma_h$ . A Cartesian coordinate system  $x/y/z$  and a cylindrical coordinate system  $r/\theta/z$  are established at the wellbore, its axes  $Oz$  is along with the wellbore axes,  $Ox$  and  $Oy$  is located on the plane normal to the borehole axes (Fig. 1). The in-situ stress components in the Cartesian coordinate system can be expressed as

$$\begin{cases} \sigma_{xx} = \sigma_H \cos^2 \alpha \cos^2 \beta + \sigma_h \cos^2 \alpha \sin^2 \beta + \sigma_v \sin^2 \alpha \\ \sigma_{yy} = \sigma_H \sin^2 \beta + \sigma_h \cos^2 \beta \\ \sigma_{zz} = \sigma_H \sin^2 \alpha \cos^2 \beta + \sigma_h \sin^2 \alpha \sin^2 \beta + \sigma_v \cos^2 \alpha \\ \sigma_{xy} = -\sigma_H \cos \alpha \cos \beta \sin \beta + \sigma_h \cos \alpha \cos \beta \sin \beta \\ \sigma_{xz} = \sigma_H \cos \alpha \sin \alpha \cos^2 \beta + \sigma_h \cos \alpha \sin \alpha \sin^2 \beta - \sigma_v \cos \alpha \sin \alpha \\ \sigma_{yz} = -\sigma_H \sin \alpha \cos \beta \sin \beta + \sigma_h \sin \alpha \cos \beta \sin \beta \end{cases} \quad (1)$$

where,  $\sigma_v$  is the overburden stress;  $\sigma_H$  and  $\sigma_h$  are the horizontal principal stresses;  $\alpha$  is the inclination;  $\beta$  is the well azimuth;  $\sigma_{xx}$ ,  $\sigma_{yy}$ ,  $\sigma_{xy}$ ,  $\sigma_{xz}$ ,  $\sigma_{yz}$  and  $\sigma_{zz}$  are the surrounding wall stress components of in the Cartesian coordinate respectively. The stresses on the wellbore wall are stated as follows (Daneshy 1973, Pearson *et al.* 1992, Abass *et al.* 1994, Hossain *et al.* 2002, Crosby *et al.* 2002, Soliman and Boonen 2002, Osorio and Lopez 2009, Fallahzadeh *et al.* 2010)

$$\begin{cases} \sigma_r = P - \phi P_n(r) \\ \sigma_\theta = -P + \sigma_{xx} + \sigma_{yy} - 2(\sigma_{xx} - \sigma_{yy}) \cos 2\theta - 4\sigma_{xy} \sin 2\theta + [\alpha(1-2\nu)/(1-\nu) - \phi]P_n(r) \\ \sigma_z = \sigma_{zz} - \nu[2(\sigma_{xx} - \sigma_{yy}) \cos 2\theta + 4\sigma_{xy} \sin 2\theta] + \delta[\alpha(1-2\nu)/(1-\nu) - \phi]P_n(r) \\ \sigma_{r\theta} = 0 \\ \sigma_{\theta z} = 2\sigma_{yz} \cos \theta - 2\sigma_{xz} \sin \theta \\ \sigma_{zr} = 0 \end{cases} \quad (2)$$

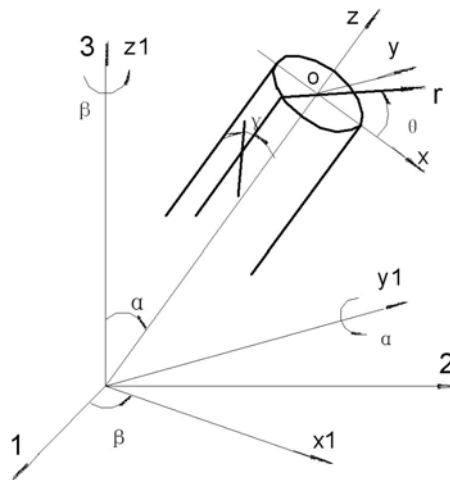


Fig. 1 Coordinates transformation of a deviated hole

The intersection of the wellbore and the perforation tunnel were simplified as a plane problem, on the basis of which the relevant stress around the intersection was obtained next, with the error of less than 2% between the theoretical solution and the corresponding one from the micro-fracturing testing (Hossain *et al.* 2002). The relevant model is shown as follows

$$\begin{cases} \sigma'_r = P - \delta\phi P_n(r) \\ \sigma'_{\theta'} = \sigma_{xx} + \sigma_{yy} + \sigma_z + 2 * (\sigma_{xx} + \sigma_{yy} - \sigma_z) \cos(2\theta') - 2(\sigma_{xx} - \sigma_{yy})(\cos(2\theta) \\ \quad + 2 \cos(2\theta) \cos(2\theta')) - 4\sigma_{xy}(1 + 2 \cos(2\theta)) \sin(2\theta) - 4\sigma_{z\theta} \sin(2\theta') \\ \quad - P(2 \cos(2\theta') + 2) + \delta[\alpha(1 - 2\nu)/(1 - \nu) - \phi]P_n(r) \\ \sigma'_z = \sigma_r - \nu[2(\sigma_z - \sigma_{\theta}) \cos 2\theta' + 4\sigma_{\theta z} \sin 2\theta'] + \delta[\alpha(1 - 2\nu)/(1 - \nu) - \phi]P_n(r) \\ \sigma'_{r\theta'} = \sigma'_{zr} = 0 \\ \sigma'_{\theta z} = 2\sigma_{r\theta} \cos \theta' - 2\sigma_{rz} \sin \theta' \end{cases} \quad (3)$$

where,  $\sigma'_r$ ,  $\sigma'_{\theta'}$ ,  $\sigma'_z$ ,  $\sigma'_{r\theta'}$ ,  $\sigma'_{zr}$  and  $\sigma'_{\theta z}$  are respectively the stresses on the perforation tunnel in the Cartesian coordinate,  $\theta'$  is the circumferential angle.

The three principal stresses on the cased well perforation tunnel wall are

$$\begin{cases} \sigma'_1 = \sigma'_r \\ \sigma'_2 = (\sigma'_z + \sigma'_{\theta'}) / 2 + \sqrt{(\sigma'_z - \sigma'_{\theta'})^2 / 4 + \sigma'_{\theta z}{}^2} \\ \sigma'_3 = (\sigma'_z + \sigma'_{\theta'}) / 2 - \sqrt{(\sigma'_z - \sigma'_{\theta'})^2 / 4 + \sigma'_{\theta z}{}^2} \end{cases} \quad (4)$$

Calculate the three principal stresses under any circumferential angle, and let the maximum principal stress be equal to the tensile strength, and then the fracture pressure of the oriented perforating cased well can be solved as

$$\begin{cases} \sigma'_3 - \alpha P_0 = S_t & \text{the tunnel wall is not permeable} \\ \sigma'_3 - \alpha P = S_t & \text{the tunnel wall is permeable} \end{cases} \quad (5)$$

Let

$$d\sigma'_3 / d\theta' = 0 \quad (6)$$

Then we can obtain the position angle  $\theta'$  of the tensile failure on the tunnel wall.

## 2.2 Hydraulic fracturing model

### 2.2.1 Seepage-deformation coupling method considering the dynamic evolvement of the reservoir porosity and permeability

The solutions of the seepage-deformation coupling can fall into two categories, namely sequential coupling and direct coupling. The sequential coupling needs two more times in order to calculate the seepage and stress fields, while the direct coupling only needs one time to calculate the coupling field by using the seepage-deformation coupling element including the whole freedom degrees of the placement and the pore pressure. In fact, the sequential coupling is a method of the cross-iteration of the seepage and stress field, so they are not coupled actually. By

contrast, the direct coupling uses the seepage-deformation coupling element and achieves the analysis without any decoupling during the analysis.

Terzaghi consolidation theory has been proved to be accurate only under the one-dimensional condition, due to the assumption that the distributions of the total stress always keep invariant during the consolidation, ignoring the change of the stress while loading, whose relevant theory in 3D is called as quasi three dimensional (pseudo-3D) consolidation theory. Combining with the strict consolidation theory, Biot (1941) proposed a three dimensional consolidation model for solid particle in the terms of the pore pressure and the deformation, often called as true three dimensional consolidation theory. In order to analyze the seepage-deformation coupling directly, the displacement-pore pressure coupling element is directly used to solve the Biot consolidation equation and obtain the analytical solutions of the coupling field in the perforation tunnels.

As a porous material, the porosity ratio of rock changes when the rock frame deforms. It can be expressed by

$$\Delta e = \Delta \left( \frac{V_p}{V_s} \right) \quad (7)$$

where,  $V_p$  is the pore volume;  $V_s$  is the solid volume. Assume that the rock particle is incompressible, and that the rock volume change is  $\Delta V = V_p$ . It can be obtained by the definition of the volumetric strain ( $\varepsilon_V = \varepsilon_x + \varepsilon_y + \varepsilon_z$ )

$$\varepsilon_V = \frac{\Delta V}{V_0} = \frac{\Delta V_p}{V_0} = \frac{V_s \Delta e}{V_s (1 + e_0)} = \frac{\Delta e}{(1 + e_0)} = \frac{e - e_0}{1 + e_0} \quad (8)$$

where,  $V_0$  is the initial volume;  $e_0$  is the initial porosity.

The relationship between the porosity and volumetric strain can be derived by Eq. (8)

$$n = 1 - \frac{1 - n_0}{\varepsilon_V} \quad (9)$$

where,  $n_0$  is the initial porosity.

The relationship between the permeability coefficient and porosity can be expressed as

$$k = \frac{\rho g}{\mu} \frac{d^2}{180} \frac{n^3}{(1 - n)^2} \quad (10)$$

where,  $k$  is the dynamic evolution permeability;  $d$  is the average diameter of solid particle.

Substituting the Eq. (9) into the Eq. (10)

$$k = k_0 \left[ \left( \frac{1}{n_0} \right) (1 + \varepsilon_V)^3 - \left( \frac{1 - n_0}{n_0} \right) (1 + \varepsilon_V)^{-1/3} \right]^3 \quad (11)$$

where,  $k_0$  is the in-situ permeability.

The user-defined subroutine can be compiled by the subroutine interface provided by the simulation software. Taking the dynamic evolution of the reservoir porosity and permeability into the consideration, and using the relationship between the permeability, porosity and the volumetric strain, the rock permeability and porosity can be obtained. They can be used as the

initial physical parameters in the next analysis, and then the volumetric strain and rock physical parameters coupling are achieved.

### 2.2.2 Hydraulic fracturing model with perforation tunnels

The element labeled as C3D38P which is a coupling hexahedral element of the displacement and the pore pressure, is adopted to mesh the formation of tunnel and the M3D4R element to mesh the casing (as shown in Fig. 2). The half of the model after removing the wellbore is shown in Fig. 2(a), and a membrane element is embedded in middle to simulate the casing. The outer diameter of model is set as 3 m, the perforation tunnel diameter 0.03 m, the wellbore diameter 0.189 m, the perforation length 0.2 m, the membrane element thickness 0.01 m, the elastic modulus 21 GPa and the Poisson ratio 0.21. The removed wellbore and perforation tunnel element is shown in Fig. 2(b). The horizontal displacement of outer cylindrical surface in the model and the displacement of the upper and down surface are restrained respectively. The pore pressure (32 MPa) is imposed on the outer cylindrical surface. After removing the wellbore, the fracturing fluid pressure and pore pressure are imposed on the perforation tunnel wall and the same fluid pressure is imposed on the membrane element inner surface. The elastic modulus for the formation is 13.8 GPa, the Poisson ratio 0.2, the tensile strength 6.0 MPa, the friction angle  $30^\circ$ , the shear angle  $10^\circ$ , the fluid penetration 20 mD, the porosity 15%, the fluid density  $1.25 \text{ g/cm}^3$ , the maximum horizontal stress 64.6 MPa, the minimum horizontal stress 52.5 MPa, the vertical stress 68.2 MPa and the formation pore pressure 32 MPa.

The solving procedures for the influence of the perforations are list below:

- In-situ stress transformation. In our study, the perforation tunnels, perpendicular to the wellbore, is used to do the simulation of the vertical well with the perforating inclined well model with different inclinations and well azimuths, by taking advantage of transformed stresses, since that the model would become so complicated that it is difficult for the mesh to generate the regular hexahedron and the grid operation, if using inclined perforation model for geometry model in FEM.

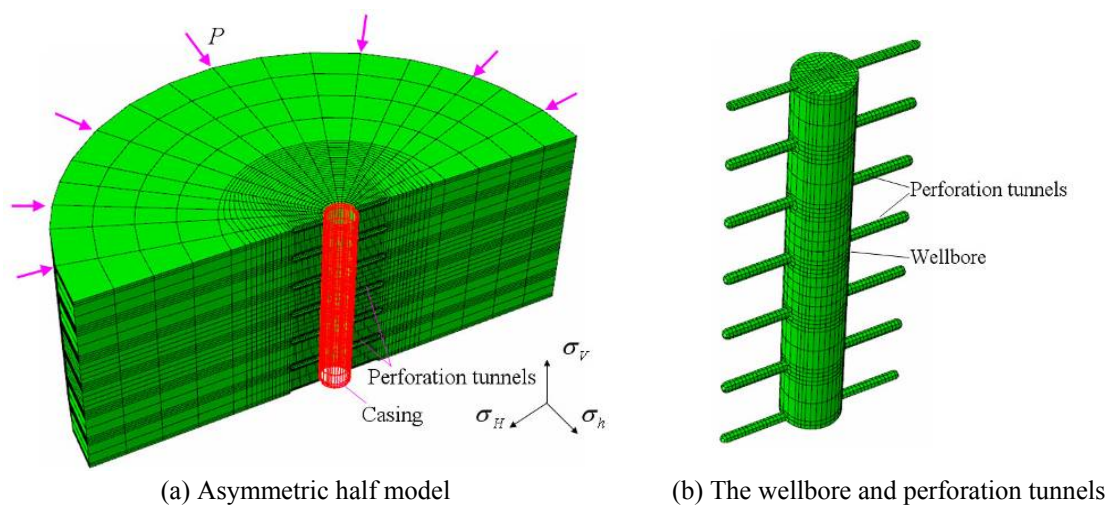


Fig. 2 Hydraulic fracturing model

- In-situ stress balance. The in-situ stresses and formation pore pressure are loaded to simulate the real in-situ stress state by the means of imposing the six in-situ stress components and the pore pressure on the rock before calculating.
- Excavation processes of the wellbore and the perforation tunnels. After the balance of the in-situ stress, the birth and death element method is adopted to do the simulation of the excavation behavior of the wellbore and the perforation tunnel at the excavation step, and then do simulation of the drilling and perforating processes, to examine the influences of the in-situ stress on the wellbore wall and the tunnel wall in the forming processes of the wellbore and the perforation tunnels.
- Hydraulic fracturing process. After the wellbore and the perforation tunnels was formed, the surface load of fluid pressure was applied to the surface of the inner wall of casing, and on the perforation tunnel wall the surface load and fluid pore pressure were applied to do the simulation of pressurized fracturing fluid process, until the formation rock fractures, namely the maximum principal stress reaches or exceeds its tensile strength. The fracturing fluid pressure at this moment is the formation fracture initiation pressure.

### 2.2.3 Model verification

In order to validate the accuracy of this mesh model, boundary condition and calculation method, the open-hole vertical well and the vertical well with a single perforation tunnel are selected to do simulation, since they have been solved with analytical solutions. The analytical initiation pressure of the open-hole well and the vertical well with a single perforation tunnel is respectively 66.9 MPa and 55.2 MPa, while the corresponding result from simulation are respectively 64.8 MPa and 57.4 MPa with the corresponding errors of 3.1% and 4.0% respectively. When the inclination is  $45^\circ$  and the azimuth is  $0^\circ$ , the analytical solution of the fracture initiation pressure of the open-hole inclined well is 65.5 MPa, and the simulation result under this condition is 67.2 MPa (Fig. 3), with the error of only 1.8% and the solution of the open-hole vertical well after the stress transformation is 66.7 MPa (Fig. 4), with the error of only 2.6%. In view of that, the transformed vertical model is working for simulating the inclined well.

The oriented perforating vertical well is the well with zero inclination, the zero well azimuth (i.e., angle with the maximum horizontal stress), and the zero orientation azimuth (i.e., angle with the maximum horizontal stress), whose perforation density is set as 12 perfs/m (perforations per

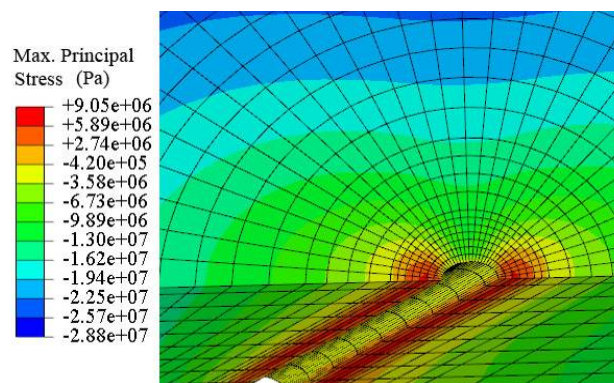


Fig. 3 The initiation pressure of the inclined open hole

meter), perforation diameter is set as 30 mm and length is set as 200 mm. The max. principal stress around the perforations can reach 6.52 MPa (Fig. 6) with the fluid pressure of 55.0 MPa (Fig. 5), while considering the casing of the casing, which has exceeded the tensile strength and was defined as formation fractures. By contrast, the maximum horizontal stress around the perforation tunnel is 5.94 MPa (Fig. 8) with the fluid pressure of 56.85 MPa (Fig. 7), which is close to the tensile strength of the formation when it is about to fracture.

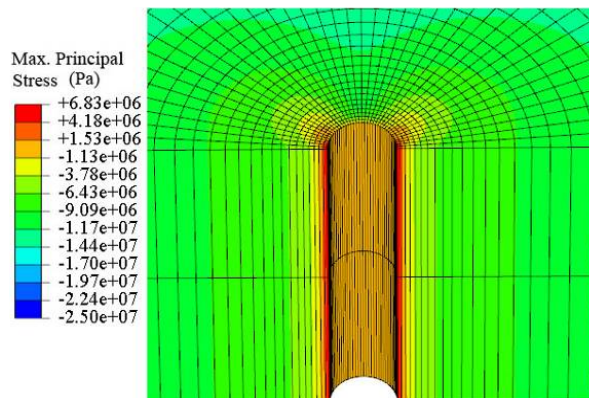


Fig. 4 The initiation pressure of the vertical open hole after the stress translation

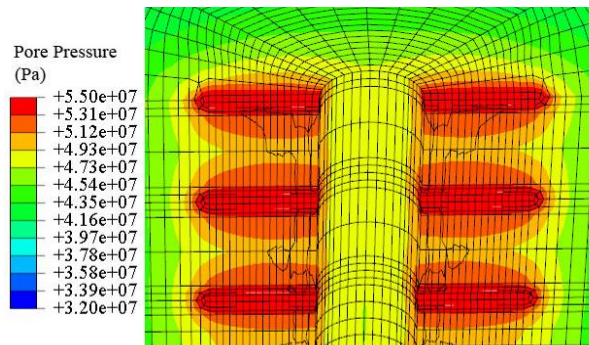


Fig. 5 The initiation pressure considering the influence of the casing

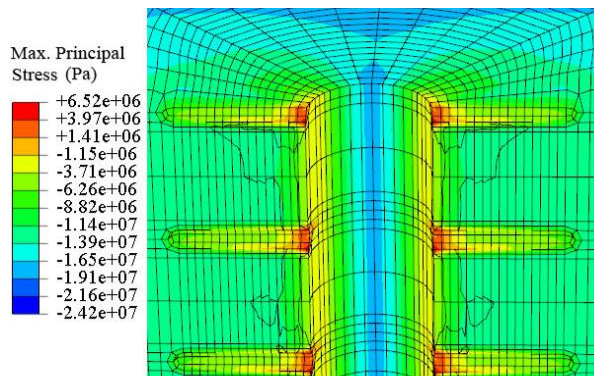


Fig. 6 The max. principal stress considering the influence of the casing

As illustrated in Fig. 7, the pore pressure around the perforation tunnel is distributed in triangle shape while considering the casing, with the maximum value in the tunnel and minimum one between the tunnels. In contrast, ignoring the presence of casing, the distribution shape of the pore pressure around the perforation tunnel is turning out to be gear tooth shape, with the gear toe in the perforation tunnel and the gear root between the tunnels. From Figs. 6 and 8, it was found that the maximum principal stress point of the perforation tunnel was located in the upper and down sides of the tunnel and is near to the casing no matter whether the casing was considered or not, which meant that the fracture will be initiated along the upper and down sides of the tunnel and is close to the casing at first, then extends along the vertical direction in the plane of the maximum principal stress, forming a big vertical plane fracture with two symmetric wings, the shape of which was matched precisely with that of the indoor hydraulic fracturing experiment and the field experiment (Daneshy 1973, El Rabaa 1989, Hallam and Last 1991).

In the analysis of the single tunnel, the maximum error of the simulation result is obtained with the maximum error of 3% comparing with the analytical initiation pressure (55.2 MPa) of is 3%, ignoring the presence of casing, while considering the presence of it may make greater improvement

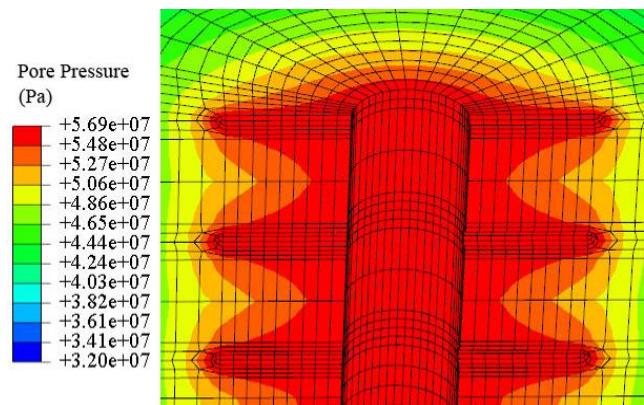


Fig. 7 The initiation pressure without considering the influence of the casing

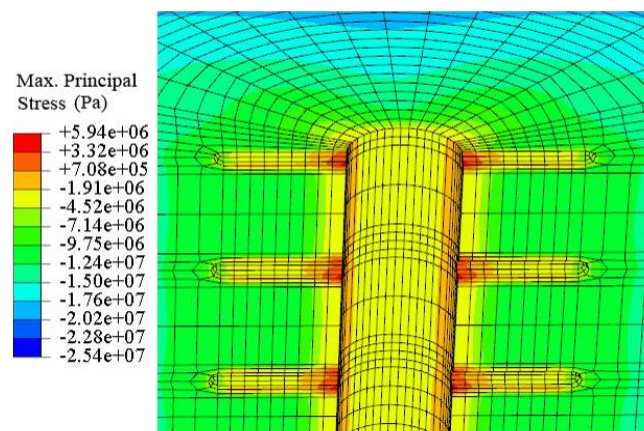


Fig. 8 The max. principal stress without considering the influence of the casing

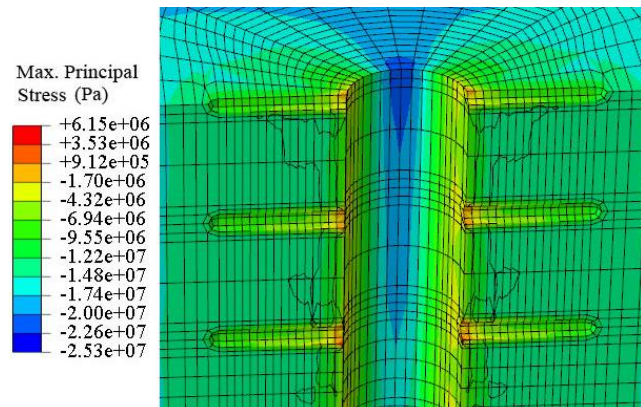


Fig. 9 The max. principal stress considering the influence of the casing after the stress translation

on the precision of simulation with the error of 0.6% between the numerical and the analytical solution. In view of that, it is necessary to consider the effects of the casing and penetration when doing numerical simulation of the reservoir initiation pressure. Considering the casing and the inclined well (the inclination is  $45^\circ$ , the well azimuth is  $0^\circ$  and the orientation azimuth is  $0^\circ$ ), the calculation result with transformed stress is shown in Fig. 9. The initiation point is still located in the upper and down sides of the tunnel on the casing wall, with the error of 4.2% between the numerical (56.4 MPa) and theoretical solution (58.9 MPa) for the initiation pressure. The results mentioned above validated the reliability and reasonability of Hossain model in the numerical simulation of the initiation pressure, which can be used to investigate the influences of the inclination and well azimuth on the initiation pressure.

### 3. Results and discussion

#### 3.1 Fracture initiation points

##### 3.1.1 Considering the influence of the casing

Fracture initiation point is located in the root of the tunnel considering the presence of casing in the simulation; the initiation point is located in the upper and down sides of the tunnel, when the perforation azimuth is set as  $0^\circ$ , with the increase of the perforation azimuth, the initiation point is moving towards the point with the maximum principal stress. Especially, when the perforation angle is  $90^\circ$ , the initiation point is located in the left and right sides of the tunnel, as shown in Fig. 10.

Hydraulic fracturing simulation experiment was carried through the  $400\text{ mm}^3$  true triaxial simulation test equipment, designed by the Rock Mechanics Laboratory of China University of Petroleum (Beijing), by setting the equivalent conditions in the experiment same with the simulation of the casing with perforation azimuth of  $45^\circ$  and  $90^\circ$  respectively. The laboratory results of field conditions are transformed by the scaling laws proposed by de Pater *et al.* (1994) to quantitatively compare with the relevant simulation result. The specimen fractures along the first row tunnel are illustrated in Fig. 11, and the process is described as follows. The fracture first happened around the perforation hole along the twisting direction of minimum horizontal stress  $\sigma_h$ ,

and then twists to  $\sigma_H$  plane perpendicular to the perforation direction, finally the twisting fractures link-up, and formed a large horizontal fracture. With the propagation of the fractures, a horizontal plane with a depressed area was formed in its middle, the outermost of the fractures twisted towards the  $\sigma_H$  direction. However, the perforations of the second and third row don't fracture at all, which are the same with that shown in Fig. 9 and was used to verify the accuracy of the numerical simulation further.

When the perforation angle is consistent with the direction of the maximum principal stress, micro-annuli between the cement sheath and formation will be produced, where the fracturing fluid would enter. The fracture initiates in the points with weakest strength around the wellbore, which meant that the direction of the initiation point may not be conformed with that of the perforation tunnel (Daneshy 1972, van de Ketterij and de Pater 1999). So we have to study the perforation initiation pressure without considering the casing.

### 3.1.2 Ignoring the influence of the casing

When the perforations are not perforated along the maximum horizontal principle stress, the mirco-annulus may be produced between cement and formation, where the fluid may enter under higher pressure. In this case, the initial fracture may be produced along the weakest orientation around wellbore, but not along the perforation orientation. That is why we also need to do some investigation of cases ignoring of effect of casing. In the following context, different results under

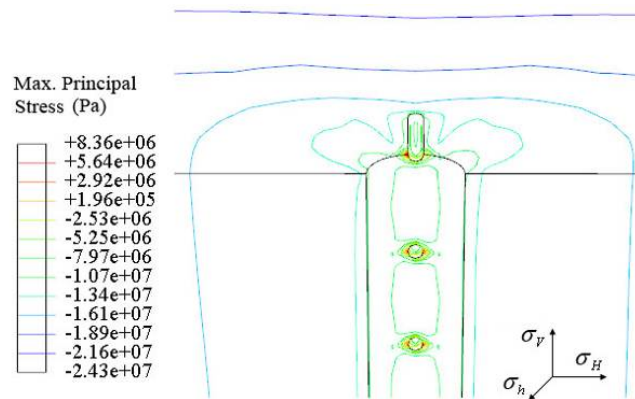


Fig. 10 The max. principal stress isoline when the perforation angle is 90°

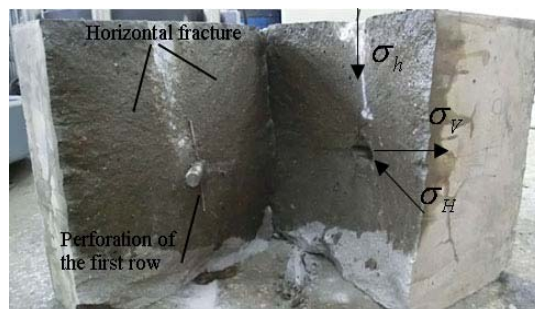


Fig. 11 Fracture propagation with 90° perforation angle

different perforation azimuth are listed to analyze the effect of casing on the initiation of fracture of wellbore under hydraulic pressure. When the perforation is  $0-15^\circ$ , the position of fracture initiation point is located at the mouth of perforation holes of wellbore, exactly on the surface of wellbore. When the perforation is  $15-30^\circ$ , the position of fracture initiation points are moving far from the surface of the wellbore (the details about that can be found in Fig. 12). When the perforation azimuth is  $45^\circ$ , stress was turning to be tension stress in the direction of the minimum principal stress along the wellbore wall (the horizontal direction in Fig. 13). When the perforation azimuth is  $45^\circ-60^\circ$ , there is a symmetric tensile area appearing in the direction of the maximum principal stress along the wellbore wall (the horizontal direction in Fig. 13), and the maximum value for the tension stress is found on the surface of the wellbore wall; the tensile area in the tunnel was continually moving away from the wellbore wall and twisted towards the direction of maximum principal stress. As shown in Fig. 13, when the perforation angle is  $60^\circ$  and there is a large tensile area appearing in both the wellbore and the perforation hole. However, the maximum principal stress in the perforation hole was slightly bigger than that on the surface of wellbore, so the fracture initiation should in the perforation hole first, and actually two fractures happened in two sides of perforation tunnels. One is located in the perforation tunnel in the vertical direction, while the other one is located in the wellbore in the direction of the maximum horizontal principal stress, which can be found in many indoor experiments for hydraulic fracturing (Daneshy 1973, El Rabaa 1989, Hallam and Last 1991, van de Ketterij and de Pater 1999). When the perforation

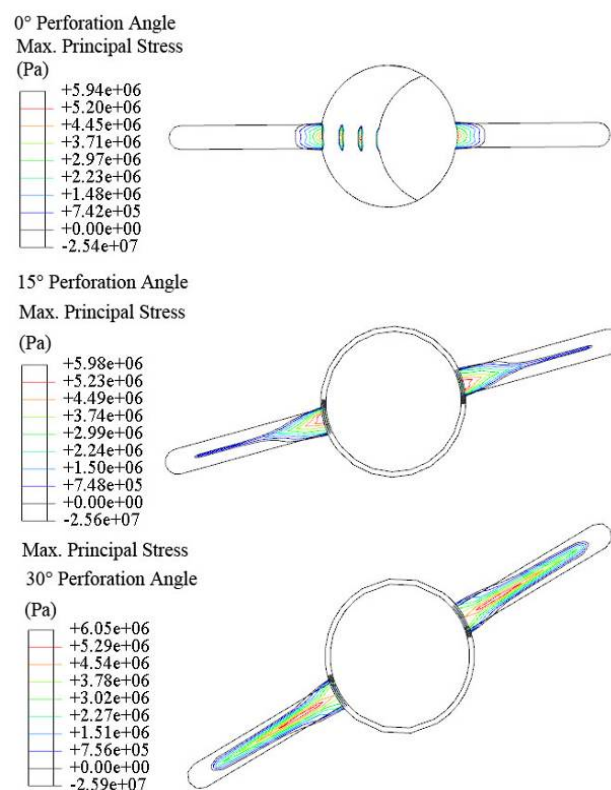


Fig. 12 The max. principal stress isoline when the perforation angle is  $0^\circ-30^\circ$

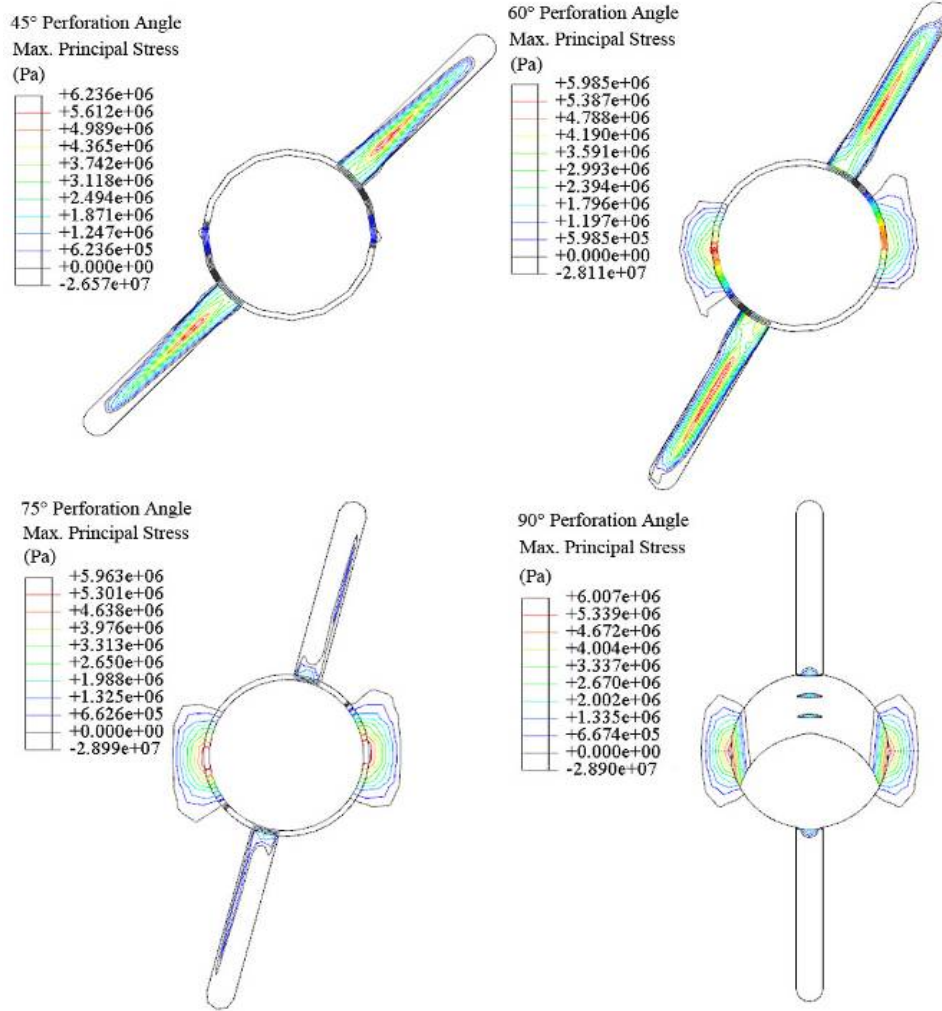


Fig. 13 The max. principal stress isoline when the perforation angle is 45°-90°

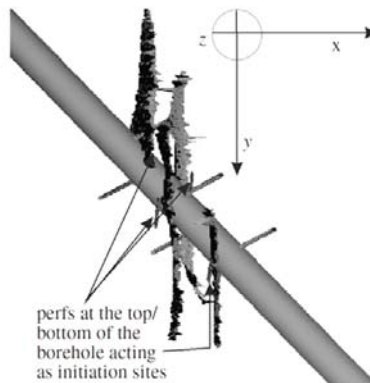


Fig. 14 There is no fracture along the tunnel when the perforation angle is 90°

angle is between  $60^\circ$  and  $90^\circ$ , the maximum principal stress on the wellbore wall is turning out to be the critical stress in the system comparing with that in perforation hole, due to great decreasing in that in the perforation hole, so the fracture is initialized and propagated in the direction of the maximum horizontal stress on the surface of wellbore, but the tunnel is intact (Fig. 13). There is nearly little tension stress in the perforation tunnel when the perforation azimuth angle is  $90^\circ$ , and the fracture initiated in the direction of the maximum horizontal principal stress in the wellbore but does not initiate in the tunnel. van de Ketterij and de Pater studied the inclined well with the azimuth of  $60^\circ$  and the inclination of  $49^\circ$ , finding that amongst the cases with the perforation angle of  $0/90/180/270^\circ$ , the case with the perforation angle of  $90^\circ$  is the only one without fracture in the formation (Fig. 14), which was also validated by our experiment (in Fig. 11). According to the above results, the assumption from Zhang *et al.* (2003) that the hydraulic fracture always initiated on the wellbore wall but not in the perforation tunnel is not quite right for the highly deviated well with large perforation angle.

### 3.1.3 Influences of well deviation and azimuth angle on fracture initiation pressure

Fig. 15 shows that there is little effect of the well deviation angle on the fracture initiation pressure, and the well deviation angle can lead to a slight increase on the fracture initiation pressure; but it increased obviously with the increase of the well azimuth angle. The results of the hydraulic fracturing simulation experiments of the medium deviated well by Hallam and Last (1991) showed: when the inclination is  $10^\circ$ ,  $20^\circ$  or  $30^\circ$ , the fracturing surface turned out to be a plane in the maximum horizontal stress direction. The conclusion is drawn that the simpler the fracture is, the lower the initiation pressure is. Therefore, the best perforation angle of the highly deviated well should be less than  $30^\circ$ .

### 3.2 Effect of the perforation density on the initiation pressure

The perforation density is represented by the number of the perforation tunnels per meter in wellbore. In this section, the perforation density ranging from 8 to 20 perfs/m is adopted to do investigation on the initiation pressure of perforation tunnels when the orientation azimuth is  $180^\circ$ , the perforation length is 200 mm, the perforation diameter is 30 mm, the inclination is  $45^\circ$ , and the well azimuth and the perforation angle are  $0^\circ$ . It is illustrated in Fig. 16 the distribution of the maximum principal stress between the tunnels is symmetrical, and the maximum principal

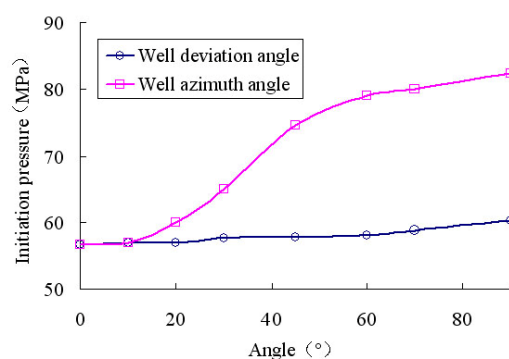


Fig. 15 The initiation pressure with different well deviation and azimuth angle

between the adjacent tunnels is located in the upper and down sides in the direction of the wellbore axis. It was shown that the perforation tunnel initiated along the vertical plane and forms a plane fracture in the direction of the maximum horizontal stress.

Fig. 17 illustrates the influences of the different perforation densities on the initiation pressure. The stress between the tunnels will be more concentrative as the perforation density increases, so the initiation pressure decreases as the perforation density increases. But the decrease is nonlinear, and this result are the same as the calculation results by Wang and Lin (1998), which further indicates the stress concentrative degrees are different because of the tunnel spacing. When the perforation density is 4~6 perfs/m or 11~15 perfs/m, the initiation pressure remains unchanged. But when the density is amongst 2~4 perfs/m, 7~10 perfs/m and 16 perfs/m, the initiation pressure decreased as the density increased. The formation tend to be more easy to fracture when the perforation density was becoming higher, but the casing strength would decrease rapidly with that and the relationship between them is expressed as follows (Zhu *et al.* 2012)

$$K = \left( 1 + \frac{fd}{2\pi(l - fd)} \left( \frac{2d}{R} + \sin \frac{2d}{R} \right) \right)^{-1} \tag{12}$$

where,  $l$  is the perforation spacing,  $d$  is the perforation diameter,  $R$  is the casing radius,  $f$  is the plastic

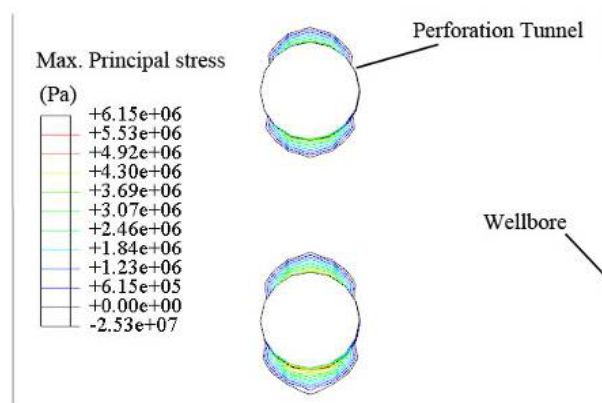


Fig. 16 The max. principal stress between the adjacent tunnels when the perforation density is 34 perfs/m

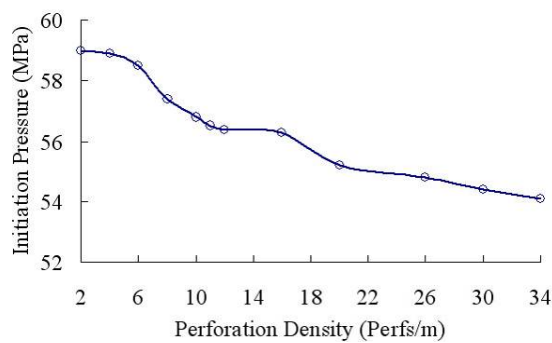


Fig. 17 The relationship of the initiation pressure and the perforation density

plastic influence coefficient. When the perforation density increases from 20 perfs/m to 34 perfs/m, the casing collapse coefficient will decrease 18.6%. So in order to determine the casing strength, we have to decrease the perforation density as much as possible. For the oriented perforation, the density of 20 perfs/m is the best for low initiation pressure but with enough casing collapse strength.

### 3.3 Effect of the perforation diameter on the initiation pressure

When the perforation length is 200 mm, the perforation density is 12 perfs/m, the inclination is 45°, and the well azimuth angle and the perforation angle are set as 0° respectively, the effects of different perforation diameters on the initiation pressure are shown in Fig. 18. Though the initiation pressure would increase as the perforation diameter increases, the influence of the perforation diameter on the initiation pressure is not that obvious. It was found in Fig. 17 that the initiation pressure reached the smallest value when the perforation diameter was set as 30 mm, so the perforation diameter of 30 mm is the best choice.

### 3.4 Effect of the perforation length on the initiation pressure

When the perforation diameter is set as 30 mm, the perforation density is 12 perfs/m, the inclination is 45°, and the well azimuth and the perforation angle are both 0°, the effect of the perforation length on the initiation pressure is shown in Fig. 19. The longer the perforation length is, the lower the initiation pressures, but the perforation length does not affect the initiation pressure too much.

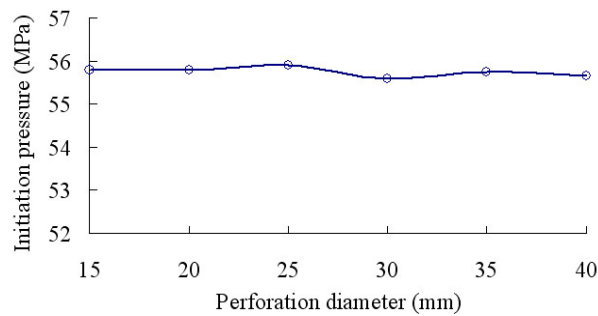


Fig. 18 The relationship of the initiation pressure and the perforation diameter

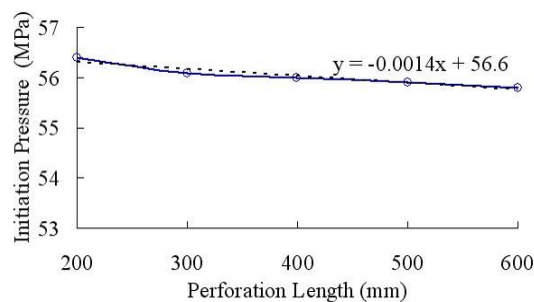


Fig. 19 The relationship of the initiation pressure and the perforation length

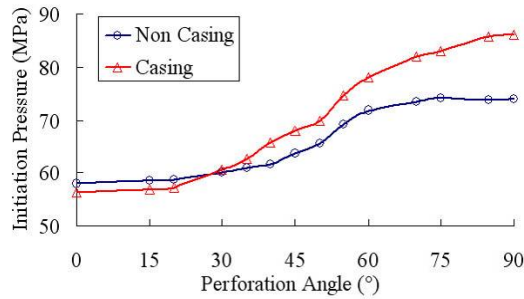


Fig. 20 The relationship of the initiation pressure and the perforation angle

### 3.5 Effect of the perforation angle on the initiation pressure

When the perforation diameter is set as 30 mm, the perforation density 12 perfs/m, the perforation length 200 mm, and the inclination 45° and the well azimuth angle 0°, the initiation pressure in both cases with and without casing, grew significantly with the increase of the perforation angles, when it is bigger than 30°, although it did not change too much when it is smaller than 30° (Fig. 20). In view of that, the perforation angle between 0°-30° are the best perforation angles for the actual drilling activity.

### 3.6 Field applications

This finite element analysis was applied for the an oilfield, whose vertical depth is about 3264 m, maximum inclination is 25° and the azimuth is 70°, with perforated casing completion (7” casing and 8-1/2” wellbore). The on-site perforation density is 20 perfs/m, the perforation length is 600 mm and the perforation tunnel diameter is 30 mm. Spiral perforating with the perforation angle of 60° was used, namely there are always two perforation tunnels located near the maximum horizontal principal stress direction, and the angle between the maximum horizontal principal stress and the two perforation tunnels is less than 30°. The Fig. 21 illustrates the on-site fracturing operation curve. The treating pressure is 64.8 MPa when the hydraulic fracture initiates. The treating pressure is the wellhead pressure, but the pressure obtained by finite element numerical simulation is the fracture initiation pressure. In order to compare them, we have to transform the wellhead pressure in the fracturing operation curve to the fracture initiation pressure. The fracture initiation pressure can be expressed as

$$P_{frac} = P_{suf} + P_{hyd} - P_{net} - P_{pf} - \Delta P_{G,P} \tag{13}$$

where,  $P_{frac}$  is the fracture initiation pressure, Pa;  $P_{suf}$  is the treating pressure, Pa;  $P_{hyd}$  is the hydrostatic fluid column pressure, Pa;  $P_{net}$  is the net pressure inside the fracture, Pa;  $P_{pf}$  is the friction loss when the fracturing fluid flows through the perforation tunnels, Pa;  $\Delta P_{G,P}$  is the friction loss when the fracturing fluid flows through the oil pipe, Pa.

- (1) The calculation equation of the friction loss produced by the perforation tunnels is (Willingham *et al.* 1993)

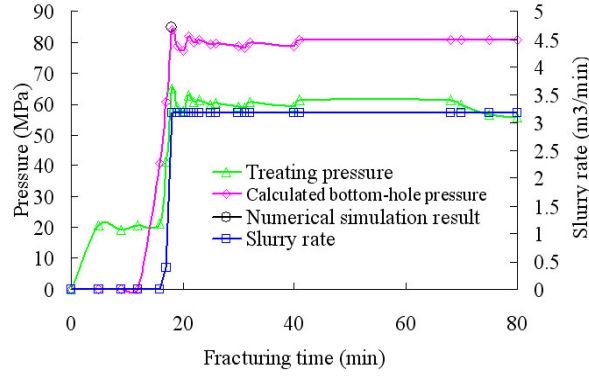


Fig. 21 The filed hydraulic fracturing operation curve of an oil-well

$$P_{pf} = 2.2326 \times 10^{-4} Q^2 \rho / (n^2 d^4 C^2) \quad (14)$$

where,  $Q$  is the slurry rate of the fracture fluid,  $\text{m}^3/\text{min}$ ;  $\rho$  is the mixed fracturing fluid density,  $\text{kg}/\text{m}^3$ ;  $n$  is the effective perforation tunnel number;  $d$  is the perforation tunnel diameter,  $\text{m}$ ;  $C$  is flow coefficient.

The calculation equation of the mixed fracturing fluid density is

$$\rho = (\rho_i + \rho_t c) / (1 + \rho_t c / \rho_s) \quad (15)$$

where,  $\rho_i$  is the base fluid density of the fracturing fluid,  $\text{kg}/\text{m}^3$ ;  $\rho_t$  is the proppant volume density, namely the ratio between the single proppant weight and the proppant accumulative body volume,  $\text{kg}/\text{m}^3$ ;  $\rho_s$  is the proppant apparent density, namely the ratio between the proppant weight and its volume,  $\text{kg}/\text{m}^3$ ;  $c$  is the proppant volume concentration, namely the ratio between the proppant accumulative body volume and the base fluid volume of fracturing fluid, non-dimensional.

The relationship between the release coefficient and the proppant weight is expressed as follows (Romero *et al.* 1995)

$$\begin{cases} C = 0.56 + 3.6376 \times 10^{-4} \rho_t \int_0^t Q(t) / ndt \\ C \leq 0.89 \end{cases} \quad (16)$$

where,  $t$  is the pump time of the sand-laden fluid,  $\text{min}$ .

- (2) For a specified well of the oilfield, the tubing above 1890 m is 3 1/2" and the tubing below 1890 m is 2-7/8". The calculation equation of the friction loss produced by the oil pipe is expressed as

$$\Delta P_{G,P} = \sigma_1 \Delta P_0^1 + \sigma_2 \Delta P_0^2 \quad (17)$$

where,  $\sigma_1$  and  $\sigma_2$  are the antifriction ratios of different size pipes, non-dimensional;  $\Delta P_0^1$  and  $\Delta P_0^2$  are the friction losses of different size clear water pipes, Pa.

$\sigma_1$ ,  $\sigma_2$ ,  $\Delta P_0^1$  and  $\Delta P_0^2$  can be respectively obtained by the following two equations (Lord and McGowen 1986)

$$\ln(1/\sigma\sigma) = 2.38 - 1.1525 \times 10^{-4} \frac{D^2}{Q} - 0.2835 \times 10^{-4} G \frac{D^2}{Q} - 0.1639 \ln \frac{G}{0.1198} - 2.3367 \times 10^{-4} P e^{0.12/G} \quad (18)$$

where,  $D$  is the pipe inner diameter, mm;  $L$  is the pipe length, m;  $G$  is the thickener concentration of the base fluid, kg/m<sup>3</sup>;  $P$  is the proppant concentration, kg/m<sup>3</sup>.

$$\Delta P_0 = 1386600 D^{-4.8} Q^{1.8} L \quad (19)$$

The flow rate of the fracturing fluid is 3.2 m<sup>3</sup>/min. The fracture fluid type is CARBO PROP. The ceramsite apparent density is 3200 Kg/m<sup>3</sup>, and the ceramsite volume density is 1900 Kg/m<sup>3</sup>. Fig. 21 shows that the fracture initiation pressure from numerical method is very close to that from the on-site fracturing operation curve with error of 1.1% between them.

The on-site microseismic monitor observed that the fracture is a plane fracture in the direction of the maximum horizontal principle stress. According to the fracturing curve, the near wellbore effect of the fracture is ignorable, indicating that the fracture initiates in the direction of the maximum horizontal principle stress, which is matched with the numerical calculation.

#### 4. Research methods

- A finite element model of the hydraulic fracturing for the perforated cased well is established on the consideration of the effect of the fluid penetration, the casing and the excavation processes of the wellbore and the perforation tunnels on the surrounding-wall stress.
- The perforation density and azimuth have great influences on the formation initiation pressure, while the perforation diameter and length have little influences on the fracture initiation pressure. The larger the perforation density and azimuth are, the higher the formation initiation pressure is. The relevant simulation results of the perforated cased well in an oilfield showed that the optimized perforation density is 20 perfs/m, the perforation diameter is 30mm and the perforation angle should be less than 30°.
- Without considering the micro-annulus but with the casing, the initiation point is always in the root of the tunnel on the wellbore wall, and the initiation point is biased to the maximum horizontal stress as the perforation angle increases. For the vertical well and the inclined well of the perforation angle less than 15° without considering the casing, the initiation point is in the root of the perforation tunnel on the wellbore wall and there are three possibilities of the initiation point for the highly deviated well with high perforation angle: when the perforation angle is 15°-45°, the initiation point is in the up side of the tunnel which is away from the wellbore wall, and the initiation point is biased toward the maximum principal stress as the perforation angle increases; when the perforation angle is 45°-60°, the initiation points are on the wellbore wall in the direction of the maximum principal stress and the upper and down sides of the perforation tunnel which is biased toward the maximum principal stress; when the perforation angle is 60°-90°, the initiation points are on the wellbore wall along the direction of the maximum principal stress and there is no fracture in the perforation tunnel.

- When using the optimized perforation parameters during the hydraulic fracturing of a well, there will be a large plane fracture, and the near wellbore effect of the fracture is feeble. The fracture initiation pressure of the well is 84.1 MPa and the finite element numerical simulation result is 85.0 MPa, they are essentially equal, which indicates that the numerical simulation method in this paper can be used to guide the on-site hydraulic fracturing design.

## Acknowledgements

Thanks to Dr. Linhua Pan for proof reading and to three unknown reviewers. This work was supported by the Science Fund for Creative Research Groups of the National Natural Science Foundation of China (51221003), the National Natural Science Foundation of China (51174219) and the Key Program of National Natural Science Foundation of China (51134004). This work was supported by the National Science and Technology Major Project of the Ministry of Science and Technology of China (No. 2011ZX05024-003-02).

## References

- Abass, H.H., Meadows, D.L., Brumley, J.L., Hedayati, S. and Venditto, J.J. (1994), "Oriented perforations - A rock mechanics view", *SPE Annual Techniesl Meeting*, New Orleans, Louisiana, September.
- Akhaveissy, A.H., Desai, C.S., Mostofinejad, D. and Vafai, A. (2013), "FE analysis of RC structures using DSC model with yield surfaces for tension and compression", *Comput. Concrete, Int. J.*, **11**(2), 123-148.
- Biao, F.J., Liu, H., Zhang, J., Zhang, S.C. and Wang, X.X. (2011), "A numerical study of fracture initiation pressure under helical perforation conditions", *J. Univ. Sci. Tech. China*, **41**(3), 219-226. [In Chinese]
- Biot, M.A. (1941), "General theory of three-dimensional consolidation", *J. Appl. Phys.*, **12**(2), 155-164.
- Cao, Z.J. and Liu, Y.Y. (2012), "A new numerical modelling for evaluating the stress intensity factors in 3-D fracture analysis", *Struct. Eng. Mech., Int. J.*, **43**(3), 321-336.
- Crosby, D.G., Rahman, M.M., Rahman, M.K. and Rahman, S.S. (2002), "Single and multiple transverse fracture initiation from horizontal wells", *J. Pet. Sci. Eng.*, **35**(3-4), 191-204.
- Daneshy, A.A. (1972), "A study of inclined hydraulic fractures", *SPE-AIME 47th Annual Fall Meeting*, San Antonio, Texas, Oct.
- Daneshy, A.A. (1973), "Experimental investigation of hydraulic fracturing through perforations", *J. Petrol. Tech.*, **25**(10), 1201-1206.
- de Pater, C.J., Cleary, M.P., Quinn, T.S., Barr, D.T., Johnson, D.E. and Weijers, L. (1994), "Experimental verification of dimensional analysis for hydraulic fracturing", *SPE Prod. Facil.*, **9**(4), 230-238.
- El Rabaa, W. (1989), "Experimental study of hydraulic fracture geometry initiated from horizontal wells", *SPE Annual Technical Conference and Exhibition*, San Antonio, Texas, October.
- Fallahzadeh, S.H., Shadizadeh, S.R., Pourafshary, P. and Zare, M.R. (2010), "Modeling the perforation stress profile for analyzing hydraulic fracture initiation in a cased hole", *Annual SPE International Conference and Exhibition*, Tinapa - Calabar, Nigeria, July-August.
- Hallam, S.D. and Last, N.C. (1991), "Geometry of hydraulic fractures from modestly deviated wellbore", *J. Petrol. Tech.*, **43**(6), 742-748.
- Hossain, M.M., Rahman, M.K. and Rahman, S.S. (2002), "Hydraulic fracture initiation and propagation: Roles of wellbore trajectory, perforation and stress regmes", *J. Petrol. Sci. Eng.*, **27**(3-4), 129-149.
- Lord, D.L. and McGowen, J.M. (1986), "Real-time treating pressure analysis aided by new correlation", *SPE Annual Technical Conference and Exhibition*, New Orleans, Louisiana, October.
- Osorio, J.G. and Lopez, C.F. (2009), "Geomechanical factors affecting the hydraulic fracturing performance in a geomechanically complex, tectonically active area in Colombia", *Latin American and Caribbean Petroleum Engineering Conference*, Cartagena de Indias, Colombia.

- Pearson, C.M., Bond, A.J., Eck, M.E. and Schmidt, J.H. (1992), "Results of stress oriented and aligned perforating in fracturing deviated wells", *J. Pet. Tech.*, **44**(1), 10-18.
- Romero, J., Mack, M.G. and Elbel, J.L. (1995), "Theoretical model and numerical investigation of near-wellbore effects in hydraulic fracturing", *SPE Annual Technical Conference and Exhibition*, Dallas, Texas, October.
- Soliman, M.Y. and Boonen, P. (2002), "Rock mechanics and stimulation aspects of horizontal wells", *J. Pet. Sci. Eng.*, **25**(3-4), 187-204.
- van de Ketterij, R.G. and de Pater, C.J. (1999), "Impact of perforations on hydraulic fracture tortuosity", *SPE Prod. Facil.*, **14**(2), 131-138.
- Wang, L.J. and Lin, J.G. (1998), "Computational complex method for finite elastic plane problem with multiple elliptical holes", *J. Basic Sci. Eng.*, **6**(4), 327-334.
- Willingham, J.D., Tan, H.C. and Norman, L.R. (1993), "Perforation friction pressure of fracturing fluid slurries", *Low Permeability Reservoirs Symposium*, Denver, Colorado, April.
- Zhang, G.Q., Chen, M., Yin, Y.Q. and Sun, H.C. (2003), "Study on influence of perforation on formation", *Chinese J. Rock Mech. Eng.*, **22**(1), 40-44. [In Chinese]
- Zhu, X.H, Liu, S.H., Tong, H., Huang, X.B. and Li, J. (2012), "Experimental and numerical study of drill pipe erosion wear in gas drilling", *Eng. Fail. Anal.*, **26**, 370-380.

CC